Deletion of Nox4 enhances remyelination following cuprizone-induced demyelination by increasing phagocytic capacity of microglia and macrophages in mice

山中, 圭

Deletion of Nox4 enhances remyelination following cuprizone-induced demyelination by increasing phagocytic capacity of microglia and macrophages in mice

Running title: Role of NOX4 in remyelination

Kei Yamanaka, Kuniyuki Nakamura, Tomoya Shibahara, Masamitsu Takashima, Hayato Takaki, Masaoki Hidaka, Motohiro Komori, Yoji Yoshikawa, Yoshinobu Wakisaka, Tetsuro Ago, Takanari Kitazono

Department of Medicine and Clinical Science, Graduate School of Medical Sciences, Kyushu University, 3-1-1 Maidashi, Higashi-ku, Fukuoka 812-8582, Japan

Acknowledgments

We thank Hideko Noguchi and Naoko Kasahara (Kyushu University) for technical support and Ryu Matsuo (Department of Health Care Administration and Management, Kyushu University) for supporting statistical analyses. We also thank Editage (www.editage.com) for English language editing. The work was supported by Grants-in-Aid for Scientific Research (B)(20H03791) (TA and TK), (C)(20K09373) (TA), (C)(19K09530) (YW) and (C)(19K09511) (KN), and Grant-in-Aid for Research Activity Start-up (21K20693) (TS)

from the Ministry of Education, Culture, Sports, Science and Technology, Japan; a grant from SENSHIN Medical Research Foundation, Japan (TA, KN, TS and YW); a grant from the Smoking Research Foundation (TA); a grant from Mochida Memorial Foundation for Medical and Pharmaceutical Research (KN); and research grants from Bayer, Boehringer Ingelheim, Bristol-Myers Squibb, Daiichi Sankyo, Eisai, MSD, and Takeda (TA and TK).

Word count: Total, 10,687; Abstract, 249; Introduction: 601; Materials and Methods: 2,105; Results: 1,906; Discussion: 1,426; Table: 3; Figures: 6; References: 66; Supplementary Figures: 2

ABSTRACT AND KEYWORDS

ABSTRACT

NOX4 is a major reactive oxygen species-producing enzyme that modulates cell stress responses. We here examined the effect of *Nox4* deletion on demyelination–remyelination, the most common pathological change in the brain. We used a model of cuprizone (CPZ)-associated demyelination–remyelination in wild-type and *Nox4*-deficient (*Nox4*$^{-/-}$) mice. While the CPZ-induced demyelination in the corpus callosum after four weeks of CPZ intoxication was slightly less pronounced in *Nox4*$^{-/-}$ mice than that in wild-type mice, remyelination following CPZ withdrawal was significantly enhanced in *Nox4*$^{-/-}$ mice with an increased accumulation of IBA1-positive microglia/macrophages in the demyelinating corpus callosum. Consistently, locomotor function, as assessed by the beam walking test, was significantly better during the remyelination phase in *Nox4*$^{-/-}$ mice. *Nox4* deletion did not affect autonomous growth of primary-culture oligodendrocyte precursor cells. Although *Nox4* expression was higher in cultured macrophages than in microglia, *Nox4*$^{-/-}$ microglia and macrophages both showed enhanced phagocytic capacity of myelin debris and produced increased amounts of trophic factors upon phagocytosis. The expression of trophic factors was higher, in parallel with the accumulation of IBA1-positive cells, in the corpus callosum in *Nox4*$^{-/-}$ mice than that in wild-type mice. *Nox4* deletion suppressed phagocytosis-induced increase in mitochondrial membrane potential, enhancing phagocytic capacity of

macrophages. Treatment with culture medium of *Nox4*$^{-/-}$ macrophages engulfing myelin debris, but not that of *Nox4*$^{-/-}$ astrocytes, enhanced cell growth and expression of myelin-associated proteins in cultured oligodendrocyte precursor cells. Collectively, *Nox4* deletion promoted remyelination after CPZ-induced demyelination by enhancing microglia/macrophage-mediated clearance of myelin debris and the production of trophic factors leading to oligodendrogenesis.

KEYWORDS: cuprizone, macrophage, microglia, Nox4, remyelination

Main Points

- Deletion of *Nox4* promotes remyelination in the brain in a cuprizone-induced mouse model of demyelination–remyelination.
- Deletion of *Nox4* promotes remyelination by enhancing microglia and macrophage phagocytic capacity and production of trophic factors.

Table of Contents Image

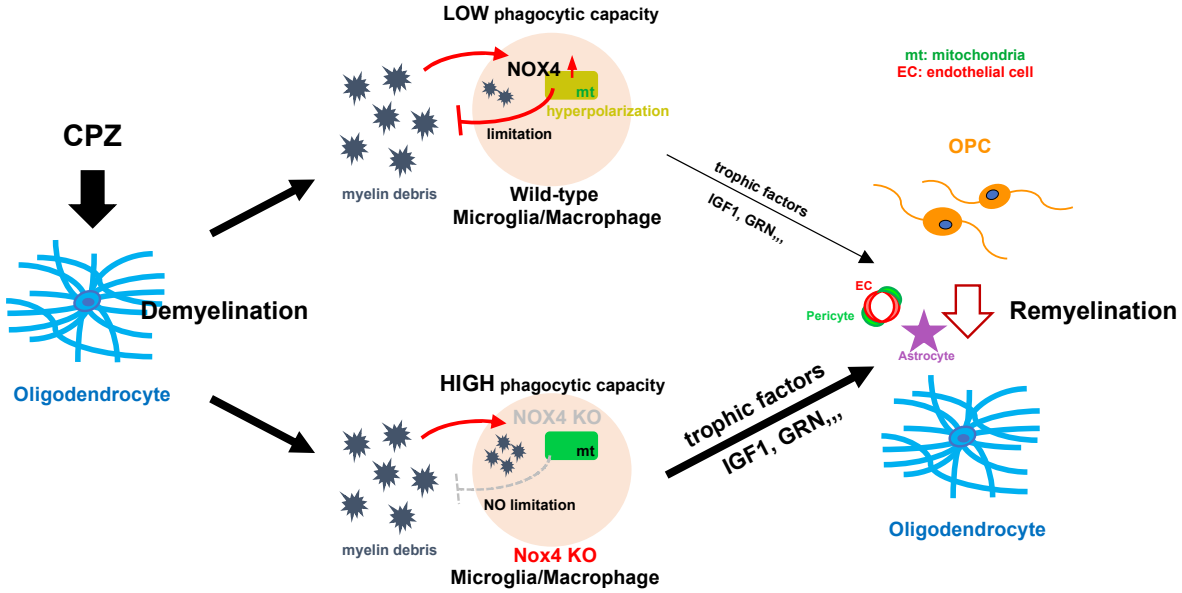

1 INTRODUCTION

Demyelination is one of the most common pathological changes in the brain. That is probably because, among neural cells, oligodendrocyte is a cell type most vulnerable to various stresses, including oxidative stress and ischemia (Dewar et al., 2003; Shi et al., 2015; Smith et al., 1999). In addition, oligodendrocytes require the support of other glial cell types, i.e., astrocytes and microglia, for differentiation and function (Hiremath et al., 1998; Liedtke et al., 1996; Menichella et al., 2003; Pang et al., 2013; Safaiyan et al., 2021). By contrast, because oligodendrocyte-mediated myelination plays a crucial role in neuronal function by providing insulation and metabolic support, demyelination can cause neuronal dysfunction and death (Funfschilling et al., 2012; Griffiths et al., 1998; Lappe-Siefke et al., 2003; Lee et al., 2012; Philips & Rothstein, 2017). Thus, maintenance of oligodendrocyte-mediated myelination is crucial for appropriate brain function.

Remyelination operates as a back-up system against demyelination in the brain. It is vital for functional recovery in various disorders of the central nervous system (CNS) accompanied by demyelination. Following demyelination, oligodendrocyte precursor cells (OPCs), which are distributed throughout the brain, proliferate and migrate to demyelinated areas, differentiate into oligodendrocytes, and produce myelin-associated proteins (Chang et al., 2002; Levine et al., 2001; Mason et al., 2000; Mi et al., 2009; Shibahara et al., 2020a). The proliferation and differentiation of OPCs, which eventually leads to remyelination, are

supported by neighboring astrocytes and appropriate blood supply (De La Fuente et al., 2017; Kipp et al., 2009; Praet et al., 2014; Skripuletz et al., 2013). Microglia- and macrophage-mediated clearance of myelin debris (MD) is prerequisite for OPC differentiation and remyelination (Hiremath et al., 1998; Kotter et al., 2005; Neumann et al., 2009; Shibahara et al., 2020b). The microglia and macrophages that engulf MD produce various trophic factors that induce OPC proliferation and differentiation, as well as astrogliosis and angiogenesis. Hence, microglia and macrophages have received much attention as key cells determining post-injury recovery in various brain disorders.

Reactive oxygen species (ROS) are key factors affecting the demyelination–remyelination processes (Nayernia et al., 2014; Smith et al., 1999). NOX4, a major ROS-producing NADPH oxidase family protein, is expressed in various cell types and is often upregulated in response to stress, such as aging, hypoxia, and malnutrition, and it accordingly modulates gene expression and cellular metabolism (Bedard & Krause, 2007). NOX4-mediated ROS production is correlated with its expression levels (Serrander et al., 2007). While apparently unaffected at baseline (Kuroda et al., 2010), mice with overexpression or deletion of *Nox4* show major phenotypic changes in various disease models, including ischemic stroke (Kleinschnitz et al., 2010; Nishimura et al., 2016), hindlimb ischemia (Craige et al., 2011), hippocampal neuroregeneration (Yoshikawa et al., 2019), atherosclerosis (Tong et al., 2016), cardiac hypertrophy and failure (Ago et al., 2010a; Kuroda et al., 2010), and diet-induced

obesity (Li et al., 2012). Interestingly, whether NOX4 is beneficial or detrimental in these scenarios depends on the disease model and phase.

In the present study, we aimed to elucidate the roles of NOX4 in the demyelination–remyelination processes. Accordingly, we established a demyelination–remyelination model in wild-type and conventional *Nox4*-deficient (*Nox4*$^{-/-}$) mice by dietary administration of cuprizone (CPZ) (Carlton, 1966; Hiremath et al., 1998; Kipp et al., 2009; Matsushima & Morell, 2001; Praet et al., 2014), and determined the effects of *Nox4* deletion on cellular and sub-cellular levels. We show that *Nox4* deletion promotes remyelination after CPZ-induced demyelination by enhancing microglia- and macrophage-mediated clearance of MD and the production of trophic factors. These findings indicate that *Nox4* inhibition in microglia and macrophages may be a potential strategy for addressing different age-related CNS disorders accompanied by demyelination.

2 MATERIALS AND METHODS

2.1 Animals

Animal experiments were conducted according to the Guidelines for Proper Conduct of Animal Experiments, published by the Science Council of Japan (June 1, 2006) (http://www.scj.go.jp/ja/info/kohyo/pdf/kohyo-20-k16-2e.pdf). The Animal Care and Use Review Committee of Kyushu University (Fukuoka, Japan) approved the animal procedures

(A21-029-4). Mice with conventional *Nox4* deletion (*Nox4*$^{-/-}$) in the C57BL/6 background were purchased from Jackson Laboratory (Bar Harbor, ME) (Yoshikawa et al., 2019). We mated male and female heterozygous Nox4 knockout mice in our facility and used male homozygous Nox4 knockout mice (*Nox4*$^{-/-}$) and their wild-type littermates as control after genetic confirmation. Mice were housed two per cage in an animal facility of Kyushu University at 21 °C and 65% humidity, with a regulated 12-h light–dark cycle and free access to food and water. Mice were randomly assigned to groups and evaluated blindly. The total number of mice used in each experiment is enlisted in **Table 1**.

2.2 CPZ intoxication

Wild-type and *Nox4*$^{-/-}$ mice (n=89 and 91 respectively; 10–12-week-old, 22–30 g) were fed a diet containing 0.2% (wt/wt) *bis*-cyclohexanone-oxalyldihydrazone (CPZ; Sigma Aldrich, #14690-25G) mixed into standard rodent chow for the indicated (2–4) weeks (Carlton, 1966; Hiremath et al., 1998). Some mice (wild-type, n=42; *Nox4*$^{-/-}$ mice, n=44) were fed a normal diet for additional one or two weeks after CPZ withdrawal to evaluate endogenous remyelination. Body weight changes during the course are shown in Figure 1(a). As described below, samples obtained from these mice were used for behavioral tests, histological analyses, and quantitative polymerase chain reaction for mRNA. We excluded eight wild-type and eight *Nox4*$^{-/-}$ mice from the analyses owing to sample preparation failure.

2.3 Locomotor function and Behavioral test

In mice, locomotor function following CPZ-induced demyelination–remyelination was assessed using the beam walking test, as reported previously (Karl et al., 2003; Skripuletz et al., 2010) with some modifications. Briefly, mice were trained to travel across a narrow beam (width 1.1 cm, length 30 cm) placed horizontally 60 cm above the floor. Each mouse was placed on one side of the beam, and a cage with straw bedding was placed on the other side. The total number of times the feet slipped off each beam was recorded for each trial. The mean values of three consecutive data were calculated. We also assessed behavioral changes using a Y-maze test. Briefly, each mouse was placed on one arm and allowed to move freely in the maze. The sequence and number of arm entries were recorded over an 8-min period. The total number of arm entries and spontaneous alternations were counted as indicators of spontaneity and working memory, respectively, as reported previously (Maki et al., 2018).

2.4 Immunohistochemistry and immunofluorescence

Mice were sacrificed on the indicated day after CPZ intoxication by intraperitoneal administration of pentobarbital (150 mg/kg body weight) and transcardially perfused with 20 mL of saline, followed by 20 ml of 4% paraformaldehyde (PFA) in phosphate-buffered saline (PBS) at 4 °C. Whole brains were fixed with 4% PFA in PBS. PFA-fixed coronal slices (2-

mm thick) were embedded in paraffin and sectioned to 4 μm. The sections were deparaffinized, rehydrated through a graded series of ethanol solutions, and washed in PBS (Tachibana et al., 2017). After blocking with a solution of 5% skimmed milk for 30 min at 25 °C, the sections were incubated with primary antibodies (**Table 2**): anti-adenomatous polyposis coli (APC) (1:100; Merck Millipore, #OP80), anti-CD13 (1:200; R&D Systems, #AF2335), anti-collagen type IV (1:100; Merck Millipore, #AB769), anti-glial fibrillary acidic protein (GFAP) (1:100; Cell Signaling Technology, #3670), anti-glutathione S-transferase π (GST-π) (1:500; MBL, #312), anti-ionized calcium-binding adapter molecule 1 (IBA1) (1:500; Abcam, #ab5076), anti-Ki-67 (1:200; Abcam, #ab15580), anti-myelin-associated glycoprotein (MAG) (1:3000; Abcam, #ab89780), anti-myelin basic protein (MBP) (1:3000; BioLegend, #808401), goat anti-oligodendrocyte transcription factor 2 (OLIG2) (1:200; R&D Systems, #AF2418), rabbit polyclonal anti-OLIG2 (1:200; Merck Millipore, #AB9610), anti-platelet derived growth factor receptor α (PDGFRα) (1:100; R&D Systems, #AF1062), and anti-proteolipid protein (PLP) (1:1000; Abcam, #ab28486) at 4 °C overnight. After washing with PBS/Triton X-100 (0.1%), the sections were incubated with appropriate secondary antibodies conjugated with Alexa Fluor dyes (1:250; Thermo Fisher Scientific, #A11029, #A11055, #A10042) in antibody diluent (DAKO, #S2022), or stained with 3,3′-diaminobenzidine (DAB) using an appropriate kit (Nichirei). For DAB staining, endogenous peroxidase was inactivated with 0.3% hydrogen peroxide for 30 min before

blocking in 5% skimmed milk solution. The stained sections were captured under the same conditions by a BZ-9000 microscope (Keyence). All sections with the same color tone were extracted with Photoshop Elements 12 software. The extracted color was then converted to grayscale and measured at the same threshold with ImageJ software 1.53. Independent persons not involved in animal procedures performed the image analysis.

2.5 Isolation of the corpus callosum

Anesthetized mice were transcardially perfused with ice-cold PBS. The brain was sectioned to obtain three 1-mm-thick coronal blocks (at 2–5 mm distance from the olfactory bulb), as previously described (Maki et al., 2018). The corpus callosum was separated under a microscope, frozen on dry ice, and stored at –80 °C until use.

2.6 Quantitative polymerase chain reaction (PCR)

Total RNA was extracted using an RNeasy lipid tissue Kit (QIAGEN, #74804) and was reverse-transcribed using a ReverTra Ace qPCR RT kit (TOYOBO, #FSQ-101). Quantitative PCR was performed using the reverse-transcription products as a template and a LightCycler 96 (Roche). We confirmed their purity by melting curves and verified their specificity by direct DNA sequencing of PCR products. The mRNA copy number was standardized using

18S rRNA as an internal control (Bas et al., 2004; Shibahara et al., 2020b). Primer sequences are shown in **Table 3**.

2.7 Cell culture

Primary cultured microglia, OPCs, and astrocytes were isolated using a mixed glial cell method from wild-type and *Nox4*$^{-/-}$ mice on postnatal days 0–3, as described previously (Shibahara et al., 2020a). Briefly, the dissected cerebral cortex was digested with papain (Sigma-Aldrich, #3125) and triturated with 60 mg/ml DNase I (Wako, #04726771). After centrifugation (200×*g*, 5 min), the cell pellet was resuspended in minimum essential medium (MEM; Gibco, #12571063) and passed through a 40 μm cell strainer (BD Falcon, #352340). After centrifugation, the mixed glial cells were suspended in Dulbecco's modified Eagle medium (DMEM) containing 10% fetal bovine serum (FBS; Gibco, #10270106) and low-concentration (0.1 ng/ml) of granulocyte-macrophage colony-stimulating factor (GM-CSF; PeproTech, #315-03), and were plated in T75 culture flasks. The medium was renewed every 2–3 d. Ten days later, microglia were detached from the astrocyte monolayer by shaking at 150 rpm for 1 h at 37 °C and were then cultured in uncoated dishes with DMEM containing 10% FBS with GM-CSF (0.1 ng/ml). OPCs, cultured without GM-CSF for 10 d, were detached from the astrocyte monolayer by shaking at 250 rpm for 16–24 h at 37 °C, and then plated in uncoated dishes to remove contaminating astrocytes and microglia. After 30-min

incubation, non-adherent OPCs were plated on 35-mm poly-L-lysine–coated dishes with DMEM with F12 supplemented with insulin (25 mg/ml; Sigma-Aldrich, #097-06474), apo-transferrin (100 mg/ml; Sigma-Aldrich, #34401-55), progesterone (20 nM; Sigma-Aldrich, #P0130), putrescine (60 μM; Sigma- Aldrich, #P5780), sodium selenite (30 nM; Sigma-Aldrich, #S5261), human platelet-derived growth factor-AA (PDGF-AA) (10 ng/ml; Peprotech, #100-13A), bFGF (20 ng/ml; Peprotech, #100-18B), and epidermal growth factor (EGF) (20 ng/ml; Peprotech, #100-15). After isolating microglia and OPCs, the remaining cells were treated with AraC (5 mM; Sigma-Aldrich, #C1768-100MG) to eliminate proliferating cells. Flasks were shaken once, and trypsin-0.05% EDTA solution (Gibco, #25300062) was added to detach astrocytes, cultured with DMEM containing 10% FBS in uncoated dishes until the cells became confluent. Human brain microvascular pericytes were purchased from ScienCell (#1200) and cultured in a pericyte medium containing 2% FBS and pericyte growth supplement (ScienCell, #1201).

Bone marrow-derived macrophages (BMDMs) were prepared from the femoral shaft of 6–8-week-old mice by flushing the femur marrow cavity with DMEM supplemented with 5% FBS. Cells were cultured in DMEM supplemented (15%) with a conditioned medium from L929 cells (a source of macrophage colony-stimulating factor) and 5% FBS (Shibahara et al., 2020b).

2.8 In vitro *cell proliferation assay*

The proliferation activity of cultured OPCs was analyzed by immunofluorescence with 5-ethynyl-2′-deoxyuridine (EdU) staining using a Click-iTTM EdU imaging kit (Thermo Fisher Scientific #A10338). Briefly, EdU (10 μ M) was added to the culture medium 24 h before fixation in 4% PFA in PBS. Fixed cells were washed with PBS and incubated with a reaction mix containing Click-iTTM reaction buffer, $CuSO_4$, Alexa Fluor 594 azide, and a reaction buffer additive for 30 min in the dark. The cells were washed once with PBS and then stained with OLIG2 antibody. EdU and OLIG2 double-positive cells were counted in five fields (200×200 μm) in each dish (n=4–5 dishes) under a fluorescence microscope (BZ-9000).

2.9 In vitro *OPC differentiation assay*

Primary OPCs were treated with astrocyte- or macrophage- conditioned medium (ACM and MCM, respectively) and OPC differentiation medium (N2 medium containing 50 ng/ml of both T3 and T4, Sigma-Aldrich, #T2877 and #T2376, respectively) at a ratio of 1:2, for 7 d. Astrocytes were cultured in DMEM containing 10% FBS in the presence or absence of MD for 48 h. When cells were treated with MD, a conditioned medium was used after centrifugation at 200×*g* for 5 min at 4 °C to remove MD. After that, MBP-positive areas against the OLIG2-positive cell number were measured using ImageJ software 1.53 (n = 5, each group).

2.10 In vitro *cell viability assay*

A cell viability assay was performed using the CellTiter96 Aqueous One Solution Cell Proliferation Assay Kit (Promega, #G3582), containing the tetrazolium dye 3-(4,5-dimethylthiazol-2-yl)-5-(3-carboxymethoxyphenyl)-2-(4-sulfophenyl)-2H-tetrazolium, inner salt (MTS), according to the manufacturer's instructions. CPZ powder was dissolved in 50% ethanol at a concentration of 1 mM under shaking at 225 rpm at 37 °C for 10–20 min until complete dissolution of the powder. Cultured pericytes were seeded in 96-well plates at a density of 5×10^3 cells/well and treated with freshly prepared CPZ (at indicated concentrations in EtOH) or EtOH alone for 72 h (Benardais et al., 2013). The One Solution Reagent was directly added to culture media; absorbance at 490 nm was recorded after incubation for 1 h.

2.11 *Immunocytochemistry*

Cells were fixed in 4% PFA in PBS for 15 min at room temperature. They were then incubated for 1 h at room temperature in a blocking solution (5% FBS and 0.3% Triton X-100) and then incubated overnight at 4 °C with the following primary antibodies: anti-OLIG2 (1:200; R&D Systems, #AF2418) and anti-MBP (MBP, 1:500; Biolegend, #808402). Stained cells were visualized under a fluorescence microscope (BZ-9000) or a confocal microscope

(Nikon A1R). The cells were counted blindly by randomly selecting five fields (200×200 μm) for each dish (n=4–5 dishes).

2.12 Oil red O (ORO) staining

MD was isolated from the brain of 10–12-week-old mice by sucrose density gradient centrifugation and was then used to stimulate cells at a concentration of 1 mg/ml of myelin protein (Shibahara et al., 2020b). The phagocytic activity of cultured microglia and BMDMs toward MD was evaluated by ORO staining. Fixed cells or frozen sections were dehydrated in 100% propylene glycol for 5 min and then stained with 0.5% ORO solution (Sigma-Aldrich, #O0625) at room temperature for 15 min. The samples were processed in 85% propylene glycol for 5 min and rinsed with distilled water three times. ORO-positive areas in the cultured microglia and BMDM were determined using at least 30 cells (Shibahara et al., 2020b). *In vivo*, ORO- and IBA1-positive cells in the corpus callosum were counted four weeks after CPZ intoxication.

2.13 Assessment of blood–brain barrier breakdown by Evans Blue dye

The permeability of the blood–brain barrier was assessed by the leakage of Evans blue dye (Sigma-Aldrich #E2129), as reported previously (Tachibana et al., 2017). The brain was collected 180 min after a 2% solution of Evans blue dye (4 mL/kg body weight) was injected

intravenously via the tail vein. After mice were euthanized and transcardially perfused with ice-cold saline, whole brains were fixed with 4% PFA in PBS and were cut into 2 mm thick coronal sections. Volumes of dye extravasation were determined by ImageJ.

2.14 Statistical analysis

The sample sizes for animal studies were determined by pilot studies or previously published works. GraphPad Prism software (version 9, La Jolla, CA) was used for statistical analyses. We verified normal distribution using the Shapiro–Wilk test. The Student's *t*-test was used to compare two groups for continuous variables with normal distributions. The differences in means among multiple groups were analyzed using one-way ANOVA, followed by a post hoc Bonferroni multiple-comparison test. Results are presented as mean ± SEM. In all analyses, $p<0.05$ was considered statistically significant.

3 RESULTS

3.1 Nox4 *deletion enhances remyelination accompanied by better recovery of locomotor function following CPZ-induced demyelination in mice*

We first compared the temporal course of CPZ-induced demyelination and spontaneous remyelination following CPZ withdrawal between wild-type and *Nox4*$^{-/-}$ mice (Figure 1(a)). Body weight changes during the course are shown in Figure 1(a): baseline body weight was

slightly heavier in *Nox4*$^{-/-}$ mice than that in wild-type mice, as reported previously (Li et al., 2012). Once body weight was reduced after the initiation of CPZ intoxication in both wild-type and *Nox4*$^{-/-}$ mice, it was restored later than two weeks in both groups. Consistent with previous reports (Hiremath et al., 1998; Kipp et al., 2009), demyelination, assessed by MBP immunostaining, was found four weeks after CPZ intoxication, in the order of the corpus callosum, the white matter, the hippocampus, and the cortex in wild-type mice (**Supplementary Figure I**); therefore, we observed CPZ-induced demyelination and remyelination and related cellular responses in the corpus callosum (yellow rectangle in Figure 1(a)) in the following experiments. Immunohistochemical analysis revealed massive demyelination, as assessed by the loss of myelinating protein MBP and GST-π–positive oligodendrocytes, in the corpus callosum four weeks after CPZ intoxication in both wild-type and *Nox4*$^{-/-}$ mice. The extent of demyelination was not significantly different between the two groups; however, remyelination following the withdrawal of CPZ was significantly greater in *Nox4*$^{-/-}$ mice than in wild-type mice (Figure 1(b,c)). We also demonstrated that remyelination, as assessed by immunostaining of PLP or MAG, was significantly greater in *Nox4*$^{-/-}$ mice than that in wild-type mice (Figure 1(d)). Quantitative PCR analysis revealed that the expression of *Mbp* and *Mag* in the corpus callosum was higher during the remyelination phase in *Nox4*$^{-/-}$ mice than that in wild-type mice (Figure 1(e)). Consistently, we found that locomotor function, as assessed by beam walking test, was significantly better

at two weeks after CPZ withdrawal in *Nox4*$^{-/-}$ mice than that in wild-type mice, although levels of impairment were similar in wild-type and *Nox4*$^{-/-}$ mice at four weeks after CPZ intoxication (Figure 1(f)). By contrast, we could not find any noticeable difference in spontaneity and working memory, as assessed by a Y-maze test, between wild-type and *Nox4*$^{-/-}$ mice, except for a slightly higher spontaneity during the remyelination phase in *Nox4*$^{-/-}$ mice (Supplementary Figure II).

3.2 OPC accumulation in the corpus callosum during the remyelination phase is greater in Nox4$^{-/-}$ *mice than that in wild-type mice*

To elucidate the mechanisms by which *Nox4* deletion enhanced remyelination, we first examined the extent of OPC accumulation in the corpus callosum in mice treated with CPZ. Immunohistochemical analysis revealed that PDGFRα-positive OPCs started to accumulate in the corpus callosum two weeks after CPZ intoxication in both wild-type and *Nox4*$^{-/-}$ mice. The accumulation was more apparent after four weeks of CPZ intoxication, during massive demyelination, and during the remyelination phase in *Nox4*$^{-/-}$ mice (Figure 2(a,b)). Similarly, the number of OLIG2-positive cells, including OPCs and oligodendrocytes, during the remyelination phase was significantly higher in *Nox4*$^{-/-}$ mice than that in wild-type mice (Figure 2(a,b)).

We then examined whether *Nox4* deletion enhanced the proliferation of primary cultured OPCs in a cell-autonomous manner. The proliferation, as assessed by EdU staining, was not significantly different between cultured OPCs prepared from *Nox4*$^{-/-}$ mice and those from wild-type mice (Figure 2(c)). We, therefore, performed double staining of anti-OLIG2/anti-Ki-67 and anti-OLIG2/anti-APC in the corpus callosum. We found that the number of OLIG2-and Ki-67 double-positive proliferating cells was significantly greater at four weeks after CPZ intoxication in *Nox4*$^{-/-}$ mice than in wild-type mice (Figure 2(d)). Furthermore, the number of OLIG2 and APC double-positive cells was also significantly greater in *Nox4*$^{-/-}$ mice than that in wild-type mice (Figure 2(d)). These findings suggested that neighboring cells other than OPCs promote the proliferation and differentiation of OPCs in the corpus callosum during the remyelination phase more greatly in *Nox4*$^{-/-}$ mice than in wild-type mice.

3.3 GFAP-positive astrogliosis and pericyte coverage of microvascular vessels are increased in the corpus callosum during the remyelination phase in Nox4$^{-/-}$ *mice*

We next examined the effects of *Nox4* deletion on the behavior of astrocytes in the corpus callosum after CPZ intoxication. Immunohistochemical analysis revealed that both groups started accumulating GFAP-positive astrocytes after approximately two weeks of CPZ intoxication. Although the extent of accumulation after four weeks of CPZ intoxication was not significantly different among the two groups, it was more significant during the

remyelination phase in *Nox4*$^{-/-}$ mice than that in wild-type mice (Figure 3(a,b)). Similarly, quantitative PCR analysis revealed that the expression of *Gfap* in the corpus callosum tended to be higher during the remyelination phase in *Nox4*$^{-/-}$ mice than that in wild-type mice (Figure 3(c)).

We then tested whether *Nox4* deletion affected the microvascular structure and function in the corpus callosum during CPZ-induced demyelination and remyelination. We first demonstrated that the treatment with CPZ neither increased the expression of NOX4 in cultured endothelial cells and pericytes nor affected the viability of pericytes (Figure 3(d)). We further confirmed that the four weeks of CPZ intoxication did not produce the impairment of the blood–brain barrier, as assessed by the leakage of Evans blue dye and the alternation of the expression changes of ZO-1 and Claudin 5, tight junction proteins, in the corpus callosum in wild-type mice (Figure 3(e)). The expression levels of the tight junction proteins following CPZ intoxication were similar between wild-type and *Nox4*$^{-/-}$ mice (Figure 3(e)), suggesting that the absence of *Nox4* did not produce the impairment of the blood–brain barrier, at least in our CPZ-induced demyelination model. Instead, microvascular density assessed by immunostaining collagen type IV, a basal membrane protein, was slightly increased at four weeks after CPZ intoxication in *Nox4*$^{-/-}$ mice compared with wild-type mice. Furthermore, microvascular density assessed by CD13-positive pericyte was significantly greater at four weeks and during the remyelination phase in *Nox4*$^{-/-}$ mice than in wild-type mice (Figure 3(f,

g)). Quantitative PCR analysis revealed that the expression of *Ng2*, a marker of neovascular pericyte (Ozerdem et al., 2001), as well as OPC (Levine et al., 2001), in the corpus callosum was significantly higher during the remyelination phase in *Nox4*$^{-/-}$ mice than in wild-type mice (Figure 3(h)). The increased number of pericyte-containing microvessels suggested better microvascular blood flow in the corpus callosum during the remyelination phase in *Nox4*$^{-/-}$ mice than in wild-type mice.

3.4 Accumulation of IBA1-positive microglia and macrophages in the corpus callosum following CPZ-induced demyelination is significantly greater in Nox4$^{-/-}$ *mice than that in wild-type mice*

We next compared the accumulation of IBA1-positive cells, i.e., microglia and macrophages, in the corpus callosum of CPZ-treated mice. Immunohistochemical analysis revealed that the accumulation of IBA1-positive cells started at 2–3 weeks and was significantly greater at four weeks in *Nox4*$^{-/-}$ mice than that in wild-type mice (Figure 4(a,b)). The IBA1 immunopositivity decreased markedly after CPZ withdrawal in both mouse groups but was slightly more pronounced during the remyelination phase in *Nox4*$^{-/-}$ mice than in wild-type mice (Figure 4(a,b)). Quantitative PCR analysis revealed that the expression of *Iba1* in the corpus callosum was significantly higher after four weeks of CPZ intoxication and during the remyelination phase in *Nox4*$^{-/-}$ mice than that in wild-type mice (Figure 4(c)). Although the

expression of *Nos2*, a marker of M1 phenotype, in the corpus callosum was not different between the two groups, that of *Arg1*, a marker of M2 phenotype, tended to be higher in *Nox4*$^{-/-}$ mice at four weeks of CPZ intoxication (Figure 4(d)) (Ransohoff, 2016). The expression of *C3*, a component of complement (Lian et al., 2016), was significantly higher during the remyelination phase in *Nox4*$^{-/-}$ mice than in wild-type mice (Figure 4(d)). Furthermore, in parallel with the *Iba1* expression, the expression of *Trem2*, *Igf1*, and *Grn* in the corpus callosum was significantly higher at four weeks (*Trem2* and *Grn*) or during the remyelination phase (*Igf1*) in *Nox4*$^{-/-}$ mice than that in wild-type mice (Figure 4(e)). Consistently, the clearance of MD, as assessed by IBA1 and ORO double staining, in the corpus callosum occurred more greatly at four weeks in *Nox4*$^{-/-}$ mice than at four weeks in wild-type mice (Figure 4(f)). Increasing accumulation of IBA1-positive microglia and macrophages may promote remyelination, possibly through enhanced clearance of MD and production of trophic factors in *Nox4*$^{-/-}$ mice.

3.5 Nox4$^{-/-}$ *microglia and macrophages more quickly engulf MD and process greater amounts of MD than wild-type cells*

To elucidate whether microglia or BMDMs contributed significantly to enhanced remyelination in *Nox4*$^{-/-}$ mice, we examined the expression levels of *Nox4* in primary cultured microglia and BMDMs prepared from C57BL/6 mice. Quantitative PCR analysis

revealed that the expression level of *Nox4* was approximately 500-fold higher in cultured BMDMs than that in microglia (Figure 5(a)). We, therefore, examined the phagocytic capacity of cultured BMDMs. Treatment with MD increased the expression of *Nox4* in wild-type BMDMs (Figure 5(b)), which was consistent with increased expression of *Nox4* in the corpus callosum following CPZ intoxication in wild-type mice (Figure 5(b)). Furthermore, immunofluorescent triple-labeling revealed that *Nox4*$^{-/-}$ BMDMs engulfed and processed more MBP-positive MD into ORO-positive lipids in 48 h than wild-type cells, with wild-type BMDMs harboring unprocessed MBP-positive MD even after 48 h (Figure 5(c)). Consistently, the extent of STAT3 phosphorylation, an indicator of phagocytosis (Campana et al., 2018), 24 h after MD treatment was significantly greater in *Nox4*$^{-/-}$ BMDMs than that in wild-type BMDMs (Figure 5(d)). Because NOX4 can localize in the inner mitochondrial membrane (Shanmugasundaram et al., 2017), we further examined the mitochondrial membrane potential changes in cells, which could affect their phagocytic capacity during MD phagocytosis (Park et al., 2011), using JC-1 dye. We found that the mitochondrial membrane potential was lower (green) and accompanied by a higher expression of *Ucp2*, an uncoupling protein, during phagocytosis in *Nox4*$^{-/-}$ macrophages than that in wild-type macrophages (Figure 5(e,f)). Further, the expression of *Igf1* and *Grn* during MD phagocytosis was significantly higher in *Nox4*$^{-/-}$ macrophages than that in wild-type cells (Figure 5(g)).

We also examined the phagocytic capacity toward MD of cultured microglia isolated from wild-type and *Nox4*$^{-/-}$ mice. Immunofluorescent triple-labeling of MBP, ORO, and Hoechst revealed that *Nox4*$^{-/-}$ microglia quickly engulfed high amounts of MBP-containing MD (within 6 h) and processed it to ORO-positive lipids within 6–24 h, which was sooner than what we observed with wild-type microglia (Figure 5(h)). Quantitative PCR analysis revealed that *Nox4*$^{-/-}$ microglia more highly expressed *Trem2*, *Igf1,* and *Grn* during MD phagocytosis than wild-type cells (Figure 5(i)). These data suggested that resident microglia may also contribute to the enhanced remyelination in *Nox4*$^{-/-}$ mice, although the expression level of *Nox4* was much lower in microglia than that in BMDM.

3.6 Nox4$^{-/-}$ *macrophages enhance the proliferation and differentiation of OPCs*

We tested whether *Nox4*$^{-/-}$ macrophages enhanced the proliferation and/or differentiation of OPCs during MD phagocytosis. Immunofluorescent labeling revealed that treatment with a culture medium of *Nox4*$^{-/-}$ BMDMs engulfing MD could significantly increase the number of OLIG2-positive OPCs and MBP-positive areas in samples compared with the treatment with a culture medium of wild-type BMDMs (Figure 6(a)). By contrast, the ability to induce the growth or MBP expression of OPCs was not significantly different between the culture media of wild-type and *Nox4*$^{-/-}$ astrocytes (Figure 6(b)). Overall, macrophages rather than astrocytes may primarily contribute to the enhanced OPC proliferation and differentiation during

remyelination in *Nox4*$^{-/-}$ mice.

4 DISCUSSION

In the current study, we investigated the roles of NOX4, a ROS-producing enzyme, in demyelination–remyelination processes in the brain. We demonstrated that *Nox4* deletion enhances remyelination following CPZ-induced demyelination in mice. The most prominent pathological change observed was the increased accumulation of IBA1-positive cells in the demyelinating corpus callosum in *Nox4*$^{-/-}$ mice. *Nox4*$^{-/-}$ cultured microglia and macrophages showed higher phagocytic capacities toward MD than wild-type cells. Finally, our data indicate that accumulated *Nox4*$^{-/-}$ microglia and macrophages enhance OPC proliferation and differentiation by enhancing the clearance of MD and the production of trophic factors. These observations position NOX4 as a molecule with important roles in brain homeostasis that could potentially be of interest as a therapeutic target in CNS disorders accompanied by demyelination.

4.1 IBA1-positive microglia and macrophages may be primarily responsible for enhanced remyelination in Nox4$^{-/-}$ *mice*

In the current study, we compared the temporal responses of glial and vascular cells during CPZ-induced demyelination and remyelination in the corpus callosum in wild-type and *Nox4*$^{-}$

$^{-/-}$ mice. PDGFRα-positive OPCs and GFAP-positive astrocytes accumulated in the corpus callosum to a similar extent in the two mouse groups prior to the occurrence of massive demyelination and the accumulation of IBA1-positive cells after four weeks of CPZ intoxication. Meanwhile, IBA1-positive cells started to accumulate in the corpus callosum after two weeks of treatment, and their accumulation was more pronounced in *Nox4*$^{-/-}$ mice than in wild-type mice after 3–4 weeks. We conclude that *Nox4* deletion primarily affected the responses of IBA1-positive cells and enhanced remyelination in a CPZ-induced demyelination model. This was also supported by the following findings: (1) *Nox4* deletion did not enhance autonomous proliferation of cultured OPCs; (2) the culture medium of *Nox4*$^{-/-}$ astrocytes did not affect OPC proliferation and differentiation, in contrast to that of *Nox4*$^{-/-}$ macrophages; (3) upon MD phagocytosis, *Nox4*$^{-/-}$ microglia and macrophages produced greater amounts of trophic factors, such as *Igf1* and *Grn*, which could lead to oligodendrogenesis, astrogliosis, and stabilization of the blood–brain barrier, than wild-type cells (Jackman et al., 2013; Kipp et al., 2009; Mason et al., 2000); and (4) the expression of these trophic factors in the corpus callosum was significantly higher in *Nox4*$^{-/-}$ mice *in vivo*, in parallel with the accumulation of IBA1-positive cells than that in wild-type mice.

The massive accumulation of IBA1-positive microglia/macrophages in the corpus callosum was reduced remarkably after CPZ withdrawal. This suggested the immediate completion of MD removal by IBA1-positive cells in the corpus callosum. By contrast,

prolonged accumulation of GFAP-positive astrocytes than IBA1-positive cells in the corpus callosum may implicate the contribution of GFAP-positive astrocytes to later remyelination processes of OPC (Matsushima & Morell, 2001; Praet et al., 2014).

4.2 NOX4 expression and phagocytic capacity in microglia and macrophages

IBA1-positive microglia and macrophages accumulate in the corpus callosum after CPZ-induced demyelination and, crucially, participate in the clearance of MD to promote remyelination (Matsushima & Morell, 2001; McMahon et al., 2002; Miron et al., 2013). NOX4 is thought to be expressed ubiquitously in various cell types (Bedard & Krause, 2007), including immortalized microglia (Li et al., 2009). Since cultured *Nox4*$^{-/-}$ microglia and macrophages both showed greater phagocytic capacity toward MD and produced greater amounts of trophic factors than wild-type cells, these two cell types may function cooperatively and enhance the remyelination processes in the corpus callosum in *Nox4*$^{-/-}$ mice. However, the *Nox4* expression level was much higher in cultured macrophages than that in microglia; therefore, macrophages, rather than microglia, may contribute more significantly to the enhanced remyelination in *Nox4*$^{-/-}$ mice. In this context, BMDMs can infiltrate into demyelinating areas without breaking the blood–brain barrier (McMahon et al., 2002). In addition, pericytes expressing CD13 and/or PDGFRβ may positively recruit BMDMs into demyelinating areas through the production of chemokines, such as MCP-1

(Shibahara et al., 2020b). Because there are no useful markers that can differentiate resident microglia and infiltrating macrophages (Bennett et al., 2016; Vankriekelsvenne et al., 2022), further experiments involving mice with microglia- or macrophage-specific deletion of *Nox4* are needed to elucidate the precise contribution of microglia and macrophages to the enhanced remyelination in *Nox4*$^{-/-}$ mice.

4.3 Putative mechanisms by which NOX4 affects phagocytic capacity of macrophages and microglia

NOX4 is often upregulated under stress conditions, such as hypoxia and aging, and modulates cellular metabolism (Ago et al., 2010b; Bedard & Krause, 2007). In the present study, *Nox4* was upregulated, at least in macrophages, upon MD phagocytosis and appeared to limit the phagocytic capacity of these cells. The mitochondrial membrane potential, which is increased upon phagocytosis, may be an important regulator of the phagocytic capacity of macrophages. For example, UCP2, a mitochondrial membrane protein that lowers the mitochondrial membrane potential, is important for continued phagocytosis by macrophages (Cereghetti & Scorrano, 2011; Park et al., 2011). Because NOX4 can localize in the inner mitochondrial membrane and may transport protons while producing ROS (Maturana et al., 2002), it may increase the mitochondrial membrane potential directly or indirectly by downregulating *UCP2* expression. We demonstrated here that, upon MD phagocytosis, the

phosphorylation of STAT3, a transcription factor that upregulates *Ucp2* expression (Hass & Barnstable, 2021), was significantly greater in *Nox4*$^{-/-}$ macrophages than in wild-type cells, although we did not determine the mechanism underlying the NOX4-mediated dephosphorylation of STAT3. Nonetheless, in support of these findings, there are reports on inverse interaction between NOX4 and UCP2 for cellular metabolism and function (Li et al., 2012; Miao et al., 2017). Although Nox4 expression was much lower in cultured microglia than that in BMDM, an increased expression of *Trem2* upon *Nox4* deletion might explain enhanced phagocytic capacity in microglia (Cignarella et al., 2020). We speculate that the aging-related decline in the phagocytic capacity of microglia/macrophages (De Maeyer & Chambers, 2021) may be explained by NOX4 expression levels in these cells because it is usually upregulated with aging (Ago et al., 2010b). Furthermore, NOX4 expression may determine the different phagocytic capacities of microglia and macrophage (in the order of: microglia > macrophage) (Baaklini et al., 2019; Galloway et al., 2019).

4.4 Significance of Nox4 *expression depends on cell type and disease model*

Phenotypic changes induced by *Nox4* expression are likely to be highly complex *in vivo*. *Nox4* expression is strongly induced in microvascular endothelial cells and pericytes during acute brain ischemia, thereby enhancing the breakdown of the blood–brain barrier (Kleinschnitz et al., 2010; Nishimura et al., 2016). However, since *Nox4*, expressed in these

cells, also promotes angiogenic responses and blood flow recovery after ischemia, it might play beneficial roles downstream of the subacute repair phase (Craige et al., 2011). Hence, we were surprised to note that *Nox4* deletion promoted the angiogenic response, accompanied by increased pericyte coverage during the remyelination phase following CPZ-induced demyelination. This was partly because CPZ did not directly injure vascular cells. Instead, *Nox4* deletion increased the production of angiogenic trophic factors, such as *Igf1* and *Grn*, in IBA-positive cells and thus might contribute to the increase in microvascular blood flow and remyelination in the corpus callosum (Jackman et al., 2013). Notably, *Nox4* expression might be induced in specific cell types, depending on the disease state, and instigate different biological responses.

4.5 Study limitations and conclusions

There are some limitations to the current study. First, we used mice with systemic deletion of *Nox4*; therefore, we could not identify which cell types were responsible for the enhanced remyelination in *Nox4*$^{-/-}$ mice. This should be tested using cell type-specific deletion of *Nox4*. Second, we only used male mice in the current study. It has been reported that CPZ-induced demyelination and remyelination occur similarly in both sexes in C57BL/6 mice (Taylor et al., 2010). While we speculated that the effects of *Nox4* deletion on the demyelination–remyelination in the CPZ model would be similar between the sexes, this

should be verified experimentally. Third, we detected only marginal phenotypic changes of behavior, as assessed in a Y-maze test, during CPZ-induced demyelination and remyelination of *Nox4*$^{-/-}$ mice. This may perhaps be caused by relatively shorter CPZ intoxication in our model (Hiremath et al., 1998).

Notwithstanding the above, in conclusion, we demonstrated that *Nox4* deletion promotes remyelination accompanied by functional recovery in the brain, most likely by enhancing phagocytic capacity of microglia and macrophages, and their production of trophic factors, in a CPZ-induced demyelination model in mice. Because demyelination is the most common pathological change in CNS disorders and *NOX4* expression increases with age and cellular stresses, NOX4 inhibition targeting microglia and macrophages may be a promising strategy in various age-related CNS disorders accompanied by demyelination.

Conflicts of Interest

The authors declare no competing financial interests.

Data Availability Statement

The data that support the findings of this study are available from the corresponding authors upon reasonable request.

REFERENCES

Ago, T., Kuroda, J., Pain, J., Fu, C., Li, H., & Sadoshima, J. (2010a). Upregulation of Nox4 by hypertrophic stimuli promotes apoptosis and mitochondrial dysfunction in cardiac myocytes. *Circ Res, 106*(7), 1253-1264. doi:10.1161/CIRCRESAHA.109.213116

Ago, T., Matsushima, S., Kuroda, J., Zablocki, D., Kitazono, T., & Sadoshima, J. (2010b). The NADPH oxidase Nox4 and aging in the heart. *Aging (Albany NY), 2*(12), 1012-1016. doi:10.18632/aging.100261

Baaklini, C. S., Rawji, K. S., Duncan, G. J., Ho, M. F. S., & Plemel, J. R. (2019). Central Nervous System Remyelination: Roles of Glia and Innate Immune Cells. *Front Mol Neurosci, 12*, 225. doi:10.3389/fnmol.2019.00225

Bas, A., Forsberg, G., Hammarstrom, S., & Hammarstrom, M. L. (2004). Utility of the housekeeping genes 18S rRNA, beta-actin and glyceraldehyde-3-phosphate-dehydrogenase for normalization in real-time quantitative reverse transcriptase-polymerase chain reaction analysis of gene expression in human T lymphocytes. *Scand J Immunol, 59*(6), 566-573. doi:10.1111/j.0300-9475.2004.01440.x

Bedard, K., & Krause, K. H. (2007). The NOX family of ROS-generating NADPH oxidases: physiology and pathophysiology. *Physiol Rev, 87*(1), 245-313. doi:10.1152/physrev.00044.2005

Benardais, K., Kotsiari, A., Skuljec, J., Koutsoudaki, P. N., Gudi, V., Singh, V., Vulinovic, F., Skripuletz, T., & Stangel, M. (2013). Cuprizone [bis(cyclohexylidenehydrazide)] is selectively toxic for mature oligodendrocytes. *Neurotox Res, 24*(2), 244-250. doi:10.1007/s12640-013-9380-9

Bennett, M. L., Bennett, F. C., Liddelow, S. A., Ajami, B., Zamanian, J. L., Fernhoff, N. B., Mulinyawe, S. B., Bohlen, C. J., Adil, A., Tucker, A., Weissman, I. L., Chang, E. F., Li, G., Grant, G. A., Hayden Gephart, M. G., & Barres, B. A. (2016). New tools for

studying microglia in the mouse and human CNS. *Proc Natl Acad Sci U S A, 113*(12), E1738-1746. doi:10.1073/pnas.1525528113

Campana, L., Starkey Lewis, P. J., Pellicoro, A., Aucott, R. L., Man, J., O'Duibhir, E., Mok, S. E., Ferreira-Gonzalez, S., Livingstone, E., Greenhalgh, S. N., Hull, K. L., Kendall, T. J., Vernimmen, D., Henderson, N. C., Boulter, L., Gregory, C. D., Feng, Y., Anderton, S. M., Forbes, S. J., & Iredale, J. P. (2018). The STAT3-IL-10-IL-6 Pathway Is a Novel Regulator of Macrophage Efferocytosis and Phenotypic Conversion in Sterile Liver Injury. *J Immunol, 200*(3), 1169-1187. doi:10.4049/jimmunol.1701247

Carlton, W. W. (1966). Response of mice to the chelating agents sodium diethyldithiocarbamate, alpha-benzoinoxime, and biscyclohexanone oxaldihydrazone. *Toxicol Appl Pharmacol, 8*(3), 512-521. doi:10.1016/0041-008x(66)90062-7

Cereghetti, G. M., & Scorrano, L. (2011). Phagocytosis: coupling of mitochondrial uncoupling and engulfment. *Curr Biol, 21*(20), R852-854. doi:10.1016/j.cub.2011.09.007

Chang, A., Tourtellotte, W. W., Rudick, R., & Trapp, B. D. (2002). Premyelinating oligodendrocytes in chronic lesions of multiple sclerosis. *N Engl J Med, 346*(3), 165-173. doi:10.1056/NEJMoa010994

Cignarella, F., Filipello, F., Bollman, B., Cantoni, C., Locca, A., Mikesell, R., Manis, M., Ibrahim, A., Deng, L., Benitez, B. A., Cruchaga, C., Licastro, D., Mihindukulasuriya, K., Harari, O., Buckland, M., Holtzman, D. M., Rosenthal, A., Schwabe, T., Tassi, I., & Piccio, L. (2020). TREM2 activation on microglia promotes myelin debris clearance and remyelination in a model of multiple sclerosis. *Acta Neuropathol, 140*(4), 513-534. doi:10.1007/s00401-020-02193-z

Craige, S. M., Chen, K., Pei, Y., Li, C., Huang, X., Chen, C., Shibata, R., Sato, K., Walsh, K., & Keaney, J. F., Jr. (2011). NADPH oxidase 4 promotes endothelial angiogenesis through endothelial nitric oxide synthase activation. *Circulation, 124*(6), 731-740. doi:10.1161/CIRCULATIONAHA.111.030775

De La Fuente, A. G., Lange, S., Silva, M. E., Gonzalez, G. A., Tempfer, H., van Wijngaarden, P., Zhao, C., Di Canio, L., Trost, A., Bieler, L., Zaunmair, P., Rotheneichner, P., O'Sullivan, A., Couillard-Despres, S., Errea, O., Mae, M. A., Andrae, J., He, L., Keller, A., Batiz, L. F., Betsholtz, C., Aigner, L., Franklin, R. J. M., & Rivera, F. J. (2017). Pericytes Stimulate Oligodendrocyte Progenitor Cell Differentiation during CNS Remyelination. *Cell Rep, 20*(8), 1755-1764. doi:10.1016/j.celrep.2017.08.007

De Maeyer, R. P. H., & Chambers, E. S. (2021). The impact of ageing on monocytes and macrophages. *Immunol Lett, 230*, 1-10. doi:10.1016/j.imlet.2020.12.003

Dewar, D., Underhill, S. M., & Goldberg, M. P. (2003). Oligodendrocytes and ischemic brain injury. *J Cereb Blood Flow Metab, 23*(3), 263-274. doi:10.1097/01.WCB.0000053472.41007.F9

Funfschilling, U., Supplie, L. M., Mahad, D., Boretius, S., Saab, A. S., Edgar, J., Brinkmann, B. G., Kassmann, C. M., Tzvetanova, I. D., Mobius, W., Diaz, F., Meijer, D., Suter, U., Hamprecht, B., Sereda, M. W., Moraes, C. T., Frahm, J., Goebbels, S., & Nave, K. A. (2012). Glycolytic oligodendrocytes maintain myelin and long-term axonal integrity. *Nature, 485*(7399), 517-521. doi:10.1038/nature11007

Galloway, D. A., Phillips, A. E. M., Owen, D. R. J., & Moore, C. S. (2019). Phagocytosis in the Brain: Homeostasis and Disease. *Front Immunol, 10*, 790. doi:10.3389/fimmu.2019.00790

Griffiths, I., Klugmann, M., Anderson, T., Yool, D., Thomson, C., Schwab, M. H., Schneider, A., Zimmermann, F., McCulloch, M., Nadon, N., & Nave, K. A. (1998). Axonal swellings and degeneration in mice lacking the major proteolipid of myelin. *Science, 280*(5369), 1610-1613. doi:10.1126/science.280.5369.1610

Hass, D. T., & Barnstable, C. J. (2021). Uncoupling proteins in the mitochondrial defense against oxidative stress. *Prog Retin Eye Res, 83*, 100941. doi:10.1016/j.preteyeres.2021.100941

Hiremath, M. M., Saito, Y., Knapp, G. W., Ting, J. P. Y., Suzuki, K., & Matsushima, G. K. (1998). Microglial/macrophage accumulation during cuprizone-induced demyelination in C57BL/6 mice. *Journal of Neuroimmunology, 92*(1-2), 38-49. doi:Doi 10.1016/S0165-5728(98)00168-4

Jackman, K., Kahles, T., Lane, D., Garcia-Bonilla, L., Abe, T., Capone, C., Hochrainer, K., Voss, H., Zhou, P., Ding, A., Anrather, J., & Iadecola, C. (2013). Progranulin deficiency promotes post-ischemic blood-brain barrier disruption. *J Neurosci, 33*(50), 19579-19589. doi:10.1523/JNEUROSCI.4318-13.2013

Karl, T., Pabst, R., & von Horsten, S. (2003). Behavioral phenotyping of mice in pharmacological and toxicological research. *Exp Toxicol Pathol, 55*(1), 69-83. doi:10.1078/0940-2993-00301

Kipp, M., Clarner, T., Dang, J., Copray, S., & Beyer, C. (2009). The cuprizone animal model: new insights into an old story. *Acta Neuropathol, 118*(6), 723-736. doi:10.1007/s00401-009-0591-3

Kleinschnitz, C., Grund, H., Wingler, K., Armitage, M. E., Jones, E., Mittal, M., Barit, D., Schwarz, T., Geis, C., Kraft, P., Barthel, K., Schuhmann, M. K., Herrmann, A. M., Meuth, S. G., Stoll, G., Meurer, S., Schrewe, A., Becker, L., Gailus-Durner, V., Fuchs, H., Klopstock, T., de Angelis, M. H., Jandeleit-Dahm, K., Shah, A. M., Weissmann, N., & Schmidt, H. H. (2010). Post-stroke inhibition of induced NADPH oxidase type 4 prevents oxidative stress and neurodegeneration. *PLoS Biol, 8*(9), e1000479. doi:10.1371/journal.pbio.1000479

Kotter, M. R., Zhao, C., van Rooijen, N., & Franklin, R. J. (2005). Macrophage-depletion induced impairment of experimental CNS remyelination is associated with a reduced oligodendrocyte progenitor cell response and altered growth factor expression. *Neurobiol Dis, 18*(1), 166-175. doi:10.1016/j.nbd.2004.09.019

Kuroda, J., Ago, T., Matsushima, S., Zhai, P., Schneider, M. D., & Sadoshima, J. (2010).

NADPH oxidase 4 (Nox4) is a major source of oxidative stress in the failing heart. *Proc Natl Acad Sci U S A, 107*(35), 15565-15570. doi:10.1073/pnas.1002178107

Lappe-Siefke, C., Goebbels, S., Gravel, M., Nicksch, E., Lee, J., Braun, P. E., Griffiths, I. R., & Nave, K. A. (2003). Disruption of Cnp1 uncouples oligodendroglial functions in axonal support and myelination. *Nat Genet, 33*(3), 366-374. doi:10.1038/ng1095

Lee, Y., Morrison, B. M., Li, Y., Lengacher, S., Farah, M. H., Hoffman, P. N., Liu, Y., Tsingalia, A., Jin, L., Zhang, P. W., Pellerin, L., Magistretti, P. J., & Rothstein, J. D. (2012). Oligodendroglia metabolically support axons and contribute to neurodegeneration. *Nature, 487*(7408), 443-448. doi:10.1038/nature11314

Levine, J. M., Reynolds, R., & Fawcett, J. W. (2001). The oligodendrocyte precursor cell in health and disease. *Trends Neurosci, 24*(1), 39-47.

Li, B., Bedard, K., Sorce, S., Hinz, B., Dubois-Dauphin, M., & Krause, K. H. (2009). NOX4 expression in human microglia leads to constitutive generation of reactive oxygen species and to constitutive IL-6 expression. *J Innate Immun, 1*(6), 570-581. doi:10.1159/000235563

Li, Y., Mouche, S., Sajic, T., Veyrat-Durebex, C., Supale, R., Pierroz, D., Ferrari, S., Negro, F., Hasler, U., Feraille, E., Moll, S., Meda, P., Deffert, C., Montet, X., Krause, K. H., & Szanto, I. (2012). Deficiency in the NADPH oxidase 4 predisposes towards diet-induced obesity. *Int J Obes (Lond), 36*(12), 1503-1513. doi:10.1038/ijo.2011.279

Lian, H., Litvinchuk, A., Chiang, A. C., Aithmitti, N., Jankowsky, J. L., & Zheng, H. (2016). Astrocyte-Microglia Cross Talk through Complement Activation Modulates Amyloid Pathology in Mouse Models of Alzheimer's Disease. *J Neurosci, 36*(2), 577-589. doi:10.1523/JNEUROSCI.2117-15.2016

Liedtke, W., Edelmann, W., Bieri, P. L., Chiu, F. C., Cowan, N. J., Kucherlapati, R., & Raine, C. S. (1996). GFAP is necessary for the integrity of CNS white matter architecture and long-term maintenance of myelination. *Neuron, 17*(4), 607-615. doi:10.1016/s0896-

6273(00)80194-4

Maki, T., Morancho, A., Martinez-San Segundo, P., Hayakawa, K., Takase, H., Liang, A. C., Gabriel-Salazar, M., Medina-Gutierrez, E., Washida, K., Montaner, J., Lok, J., Lo, E. H., Arai, K., & Rosell, A. (2018). Endothelial Progenitor Cell Secretome and Oligovascular Repair in a Mouse Model of Prolonged Cerebral Hypoperfusion. *Stroke, 49*(4), 1003-1010. doi:10.1161/STROKEAHA.117.019346

Mason, J. L., Jones, J. J., Taniike, M., Morell, P., Suzuki, K., & Matsushima, G. K. (2000). Mature oligodendrocyte apoptosis precedes IGF-1 production and oligodendrocyte progenitor accumulation and differentiation during demyelination/remyelination. *J Neurosci Res, 61*(3), 251-262. doi:10.1002/1097-4547(20000801)61:3<251::AID-JNR3>3.0.CO;2-W

Matsushima, G. K., & Morell, P. (2001). The neurotoxicant, cuprizone, as a model to study demyelination and remyelination in the central nervous system. *Brain Pathology, 11*(1), 107-116.

Maturana, A., Krause, K. H., & Demaurex, N. (2002). NOX family NADPH oxidases: do they have built-in proton channels? *J Gen Physiol, 120*(6), 781-786. doi:10.1085/jgp.20028713

McMahon, E. J., Suzuki, K., & Matsushima, G. K. (2002). Peripheral macrophage recruitment in cuprizone-induced CNS demyelination despite an intact blood-brain barrier. *J Neuroimmunol, 130*(1-2), 32-45. doi:10.1016/s0165-5728(02)00205-9

Menichella, D. M., Goodenough, D. A., Sirkowski, E., Scherer, S. S., & Paul, D. L. (2003). Connexins are critical for normal myelination in the CNS. *J Neurosci, 23*(13), 5963-5973.

Mi, S., Miller, R. H., Tang, W., Lee, X., Hu, B., Wu, W., Zhang, Y., Shields, C. B., Zhang, Y., Miklasz, S., Shea, D., Mason, J., Franklin, R. J., Ji, B., Shao, Z., Chedotal, A., Bernard, F., Roulois, A., Xu, J., Jung, V., & Pepinsky, B. (2009). Promotion of central nervous

system remyelination by induced differentiation of oligodendrocyte precursor cells. *Ann Neurol, 65*(3), 304-315. doi:10.1002/ana.21581

Miao, Y., Dong, Y., Huang, P., Zhao, X., Huang, Z., Yao, J., Li, H., & Xu, Q. (2017). Increasing UCP2 expression and decreasing NOX1/4 expression maintain chondrocyte phenotype by reducing reactive oxygen species production. *Oncotarget, 8*(38), 63750-63763. doi:10.18632/oncotarget.18908

Miron, V. E., Boyd, A., Zhao, J. W., Yuen, T. J., Ruckh, J. M., Shadrach, J. L., van Wijngaarden, P., Wagers, A. J., Williams, A., Franklin, R. J. M., & Ffrench-Constant, C. (2013). M2 microglia and macrophages drive oligodendrocyte differentiation during CNS remyelination. *Nat Neurosci, 16*(9), 1211-1218. doi:10.1038/nn.3469

Nayernia, Z., Jaquet, V., & Krause, K. H. (2014). New insights on NOX enzymes in the central nervous system. *Antioxid Redox Signal, 20*(17), 2815-2837. doi:10.1089/ars.2013.5703

Neumann, H., Kotter, M. R., & Franklin, R. J. (2009). Debris clearance by microglia: an essential link between degeneration and regeneration. *Brain, 132*(Pt 2), 288-295. doi:10.1093/brain/awn109

Nishimura, A., Ago, T., Kuroda, J., Arimura, K., Tachibana, M., Nakamura, K., Wakisaka, Y., Sadoshima, J., Iihara, K., & Kitazono, T. (2016). Detrimental role of pericyte Nox4 in the acute phase of brain ischemia. *J Cereb Blood Flow Metab, 36*(6), 1143-1154. doi:10.1177/0271678X15606456

Ozerdem, U., Grako, K. A., Dahlin-Huppe, K., Monosov, E., & Stallcup, W. B. (2001). NG2 proteoglycan is expressed exclusively by mural cells during vascular morphogenesis. *Dev Dyn, 222*(2), 218-227. doi:10.1002/dvdy.1200

Pang, Y., Fan, L. W., Tien, L. T., Dai, X., Zheng, B., Cai, Z., Lin, R. C., & Bhatt, A. (2013). Differential roles of astrocyte and microglia in supporting oligodendrocyte development and myelination in vitro. *Brain Behav, 3*(5), 503-514. doi:10.1002/brb3.152

Park, D., Han, C. Z., Elliott, M. R., Kinchen, J. M., Trampont, P. C., Das, S., Collins, S., Lysiak, J. J., Hoehn, K. L., & Ravichandran, K. S. (2011). Continued clearance of apoptotic cells critically depends on the phagocyte Ucp2 protein. *Nature, 477*(7363), 220-224. doi:10.1038/nature10340

Philips, T., & Rothstein, J. D. (2017). Oligodendroglia: metabolic supporters of neurons. *J Clin Invest, 127*(9), 3271-3280. doi:10.1172/JCI90610

Praet, J., Guglielmetti, C., Berneman, Z., Van der Linden, A., & Ponsaerts, P. (2014). Cellular and molecular neuropathology of the cuprizone mouse model: clinical relevance for multiple sclerosis. *Neurosci Biobehav Rev, 47*, 485-505. doi:10.1016/j.neubiorev.2014.10.004

Ransohoff, R. M. (2016). A polarizing question: do M1 and M2 microglia exist? *Nat Neurosci, 19*(8), 987-991. doi:10.1038/nn.4338

Safaiyan, S., Besson-Girard, S., Kaya, T., Cantuti-Castelvetri, L., Liu, L., Ji, H., Schifferer, M., Gouna, G., Usifo, F., Kannaiyan, N., Fitzner, D., Xiang, X., Rossner, M. J., Brendel, M., Gokce, O., & Simons, M. (2021). White matter aging drives microglial diversity. *Neuron, 109*(7), 1100-1117 e1110. doi:10.1016/j.neuron.2021.01.027

Serrander, L., Cartier, L., Bedard, K., Banfi, B., Lardy, B., Plastre, O., Sienkiewicz, A., Forro, L., Schlegel, W., & Krause, K. H. (2007). NOX4 activity is determined by mRNA levels and reveals a unique pattern of ROS generation. *Biochem J, 406*(1), 105-114. doi:10.1042/BJ20061903

Shanmugasundaram, K., Nayak, B. K., Friedrichs, W. E., Kaushik, D., Rodriguez, R., & Block, K. (2017). NOX4 functions as a mitochondrial energetic sensor coupling cancer metabolic reprogramming to drug resistance. *Nat Commun, 8*(1), 997. doi:10.1038/s41467-017-01106-1

Shi, H., Hu, X., Leak, R. K., Shi, Y., An, C., Suenaga, J., Chen, J., & Gao, Y. (2015). Demyelination as a rational therapeutic target for ischemic or traumatic brain injury.

Exp Neurol, 272, 17-25. doi:10.1016/j.expneurol.2015.03.017

Shibahara, T., Ago, T., Nakamura, K., Tachibana, M., Yoshikawa, Y., Komori, M., Yamanaka, K., Wakisaka, Y., & Kitazono, T. (2020a). Pericyte-Mediated Tissue Repair through PDGFRβ Promotes Peri-Infarct Astrogliosis, Oligodendrogenesis, and Functional Recovery after Acute Ischemic Stroke. *eNeuro, 7*(2), ENEURO.0474-0419.2020. doi:10.1523/ENEURO.0474-19.2020

Shibahara, T., Ago, T., Tachibana, M., Nakamura, K., Yamanaka, K., Kuroda, J., Wakisaka, Y., & Kitazono, T. (2020b). Reciprocal Interaction Between Pericytes and Macrophage in Poststroke Tissue Repair and Functional Recovery. *Stroke, 51*(10), 3095-3106. doi:10.1161/STROKEAHA.120.029827

Skripuletz, T., Hackstette, D., Bauer, K., Gudi, V., Pul, R., Voss, E., Berger, K., Kipp, M., Baumgartner, W., & Stangel, M. (2013). Astrocytes regulate myelin clearance through recruitment of microglia during cuprizone-induced demyelination. *Brain, 136*(Pt 1), 147-167. doi:10.1093/brain/aws262

Skripuletz, T., Miller, E., Moharregh-Khiabani, D., Blank, A., Pul, R., Gudi, V., Trebst, C., & Stangel, M. (2010). Beneficial effects of minocycline on cuprizone induced cortical demyelination. *Neurochem Res, 35*(9), 1422-1433. doi:10.1007/s11064-010-0202-7

Smith, K. J., Kapoor, R., & Felts, P. A. (1999). Demyelination: the role of reactive oxygen and nitrogen species. *Brain Pathol, 9*(1), 69-92. doi:10.1111/j.1750-3639.1999.tb00212.x

Tachibana, M., Ago, T., Wakisaka, Y., Kuroda, J., Shijo, M., Yoshikawa, Y., Komori, M., Nishimura, A., Makihara, N., Nakamura, K., & Kitazono, T. (2017). Early Reperfusion After Brain Ischemia Has Beneficial Effects Beyond Rescuing Neurons. *Stroke, 48*(8), 2222-2230. doi:10.1161/STROKEAHA.117.016689

Taylor, L. C., Gilmore, W., Ting, J. P., & Matsushima, G. K. (2010). Cuprizone induces similar demyelination in male and female C57BL/6 mice and results in disruption of the estrous cycle. *J Neurosci Res, 88*(2), 391-402. doi:10.1002/jnr.22215

Tong, X., Khandelwal, A. R., Wu, X., Xu, Z., Yu, W., Chen, C., Zhao, W., Yang, J., Qin, Z., Weisbrod, R. M., Seta, F., Ago, T., Lee, K. S., Hammock, B. D., Sadoshima, J., Cohen, R. A., & Zeng, C. (2016). Pro-atherogenic role of smooth muscle Nox4-based NADPH oxidase. *J Mol Cell Cardiol, 92*, 30-40. doi:10.1016/j.yjmcc.2016.01.020

Vankriekelsvenne, E., Chrzanowski, U., Manzhula, K., Greiner, T., Wree, A., Hawlitschka, A., Llovera, G., Zhan, J., Joost, S., Schmitz, C., Ponsaerts, P., Amor, S., Nutma, E., Kipp, M., & Kaddatz, H. (2022). Transmembrane protein 119 is neither a specific nor a reliable marker for microglia. *Glia, 70*(6), 1170-1190. doi:10.1002/glia.24164

Yoshikawa, Y., Ago, T., Kuroda, J., Wakisaka, Y., Tachibana, M., Komori, M., Shibahara, T., Nakashima, H., Nakashima, K., & Kitazono, T. (2019). Nox4 Promotes Neural Stem/Precursor Cell Proliferation and Neurogenesis in the Hippocampus and Restores Memory Function Following Trimethyltin-Induced Injury. *Neuroscience, 398*, 193-205. doi:10.1016/j.neuroscience.2018.11.046

TABLE 1 Animal use

Experiment	Model	Sacrifice schedule	Numbers analyzed/used	Body weight	Age (weeks)
Immunohistchemistry	Wild-type, Control	day28	10/10	26.9±1.4	11.5±0.8
	Nox4$^{-/-}$, Control	day28	10/10	27.6±1.2	11.0±0.7
	Wild-type, CPZ	day14	5/7*	27.5±1.3	11.6±0.4
	Nox4$^{-/-}$, CPZ	day14	5/5	27.7±1.0	11.7±0.3
	Wild-type, CPZ	day21	5/6*	27.3±1.3	11.8±0.2
	Nox4$^{-/-}$, CPZ	day21	4/6*	26.7±1.7	11.4±0.4
	Wild-type, CPZ	day28	8/8	26.6±1.0	11.2±1.1
	Nox4$^{-/-}$, CPZ	day28	8/9*	27.2±1.0	11.1±0.5
	Wild-type, CPZ(4w)+CPZ withdrawal(1w)	day35	5/6*	25.4±1.9	10.4±0.4
	Nox4$^{-/-}$, CPZ(4w)+CPZ withdrawal(1w)	day35	5/6*	27.9±2.1	11.6±0.3
	Wild-type, CPZ(4w)+CPZ withdrawal(2w)	day42	17/19*	26.5±1.1	11.1±0.7
	Nox4$^{-/-}$, CPZ(4w)+CPZ withdrawal(2w)	day42	17/19*	27.8±1.1	11.3±0.9
	subtotal		99/111		
Triple immunofluorescence	Wild-type, CPZ	day28	4/4	26.7±1.7	11.4±0.6
	Nox4$^{-/-}$, CPZ	day28	4/4	27.4±1.5	11.1±0.8
	subtotal		8/8		
Behavioral analysis	Wild-type, Control	day42	5/5	27.1±1.1	11.1±0.5
	Nox4$^{-/-}$, Control	day42	5/5	27.3±1.0	10.9±0.5
	Wild-type, CPZ	day28	17/17	26.4±1.7	11.2±0.7
	Nox4$^{-/-}$, CPZ	day28	18/18	27.7±1.5	11.3±0.9
	Wild-type, CPZ+followed by Normal feeding	day42	10/10	27.2±1.4	11.1±0.8
	Nox4$^{-/-}$, CPZ+followed by Normal feeding	day42	12/12	28.0±1.5	10.8±0.9
	subtotal		67/67		
RNA sample	Wild-type, Control	day28	5/6*	27.3±1.0	11.5±0.5
	Nox4$^{-/-}$, Control	day28	4/6*	27.1±1.3	10.7±0.5
	Wild-type, CPZ	day28	5/5	26.8±1.1	10.5±0.3
	Nox4$^{-/-}$, CPZ	day28	5/5	28.8±0.8	11.3±0.5
	Wild-type, CPZ+followed by Normal feeding	day42	6/7*	26.2±0.8	10.2±0.3
	Nox4$^{-/-}$, CPZ+followed by Normal feeding	day42	7/7	28.0±1.0	10.8±0.2
	subtotal		32/36		
Microglia sample	Wild-type		16/16	26.2±1.7	11.7±0.8
	Nox4$^{-/-}$		16/16	27.8±1.8	11.0±1.0
	subtotal		32/32		
OPC/Astrocyte sample	Wild-type		16/16	26.8±1.3	10.7±0.9
	Nox4$^{-/-}$		16/16	27.5±1.7	10.5±0.6
	subtotal		32/32		
BMDM sample	Wild-type		6	26.7±1.9	11.3±0.5
	Nox4$^{-/-}$		6	28.0±0.8	11.6±0.3
	subtotal		12/12		
	total		282/298		
Exclusion criteria: *Failure of sample preparation.					

TABLE 2 Antibodies used for immunostaining and immunoblot analysis

Primary antibody	source	Catalog Number	RRID	Application	Reference
Mouse monoclonal anti-APC	Calbiochem	OP80	AB_2057371	Immunofluorescence	doi:10.1523/ENEURO.0474-19.2020
Goat polyclonal anti-CD13	R&D Systems	AF2335	AB_2227288	Immunofluorescence	doi: 10.1083/jcb.201807178
Goat polyclonal anti-Collagen type IV	Merck Millipore	AB769	AB_11210995	Immunofluorescence	doi: 10.1083/jcb.201807178
Mouse monoclonal anti-GFAP	Cell Signaling Technology	3670	AB_561049	Immunofluorescence	doi: 10.1161/STROKEAHA.117.016689
Rabbit polyclonal anti-GST π	MBL	312	AB_591792	Immunofluorescence	doi: 10.1523/jneurosci.6344-10.2011
Goat polyclonal anti-IBA1	abcam	ab5076	AB_2224402	Immunofluorescence	doi: 10.1016/j.neuron.2018.12.010
Rabbit polyclonal anti-Ki67	abcam	ab15580	AB_443209	Immunofluorescence	doi: 10.1002/glia.23937
Mouse monoclonal anti-MAG	abcam	ab89780	AB_2042411	Immunofluorescence	doi: 10.1186/s40478-020-01105-2
Mouse monoclonal anti-MBP	BioLegend	808401	AB_2564741	Immunofluorescence	doi: 10.1038/s41593-018-0278-y
Goat polyclonal anti-OLIG2	R&D Systems	AF2418	AB_2157554	Immunofluorescence	doi:10.1523/ENEURO.0474-19.2020
Rabbit polyclonal anti-OLIG2	Merck Millipore	AB9610	AB_570666	Immunofluorescence	doi: 10.1002/brb3.174
Goat polyclonal anti-PDGFR α	R&D Systems	AF1062	AB_2236897	Immunofluorescence	doi: 10.1038/srep08468
Mouse monoclonal anti-PLP	abcam	ab28486	AB_776593	Immunofluorescence	doi: 10.7554/eLife.30498
Mouse monoclonal anti- β -actin	Sigma	5441	AB_476744	Immunoblot analysis	doi: 10.1016/j.brainres.2019.05.020
Rabbit monoclonal anti-STAT3	Cell Signaling Technology	4904	AB_331269	Immunoblot analysis	doi: 10.1161/STROKEAHA.120.029827
Rabbit monoclonal anti-Phospho-STAT3(Tyr705)	Cell Signaling Technology	9145	AB_2491009	Immunoblot analysis	doi: 10.1161/STROKEAHA.120.029827

TABLE 3 Primers used for PCR

Mouse-specific primers		
Target gene (accession number)	Forward (5'–3')	Reverse (5'–3')
Arg1（NM_007482)	GGAATCTGCATGGGCAACCTGTGT	AGGGTCTACGTCTCGCAAGCCA
C3 (NM_009778)	TCCAACAAGAACACCCTCA	GGCTGGATAAGTCCCACA
Gfap (NM_010277)	AAGGTTGAATCGCTGGAGGA	AAGGTTGAATCGCTGGAGGA
Grn (NM_008175)	TGGTTCACACACGATGCGTTTCAC	AAAGGCAAAGACACTGCCCTGTTG
Iba1 (NM_019467)	GGATCTGCCGTCCAAACTTG	CCAGTTGGCCTCTTGTGTTC
Igf1 (NM_010512)	TGGATGCTCTTCAGTTCGTG	GTCTTGGGCATGTCAGTGTG
Mag (NM_010758)	TGCTCACCAGCATCCTCACG	AGCAGCCTCCTCTCAGATCC
Mbp (NM_010777)	TACCTGGCCACAGCAAGTAC	GTCACAATGTTCTTGAAG
Ng2 (NM_139001)	GCACGATGACTCTGAGACCA	AGCATCGCTGAAGGCTACAT
Nos2 (NM_010927)	GGCAGCCTGTGAGACCTTTG	CATTGGAAGTGAAGCGTTTCG
Nox4 (NM_015760)	ACAGAAGGTCCCTAGCAGGAG	CTGAAAAGTTGAGGGCATTCACC
Pdgfrb (NM_008809)	CACCTTCTCCAGTGTGCTGA	GGAGTCCATAGGGAGGAAGC
Trem2 (NM_031254)	TGGGACCTCTCCACCAGTT	GTGGTGTTGAGGGCTTGG
Ucp2 (NM_011671)	GCGTTCTGGGTACCATCCTA	GCTCTGAGCCCTTGGTGTAG
18S rRNA	AAACGGCTACCACATCCAAG	CCTCCAATGGATCCTCGTTA
Human-specific primers		
Target gene (accession number)	Forward (5'–3')	Reverse (5'–3')
NG2	GCACGATGACTCTGAGACCA	AGCATCGCTGAAGGCTACAT
NOX4	GGATGACTGGAAACCATACA	CTGTTTGACTGAGGTACAGC
PDGFRB	AGGTGGTTGCACATTTGTCCAG	TGTGCAGCTGTGTTCTTGAGAC
18S rRNA	AAACGGCTACCACATCCAAG	CCTCCAATGGATCCTCGTTA

Figure Legends

FIGURE 1 Remyelination following cuprizone (CPZ)-induced demyelination is enhanced in *Nox4*$^{-/-}$ mice. (a) Experimental scheme. Wild-type or *Nox4*$^{-/-}$ mice were fed CPZ mixed with a standard rodent chow for 4 weeks, and then standard chow for additional 2 weeks. Tissue histology and protein expression in the corpus callosum (yellow rectangle) were evaluated after 0 (control), 2, 3, and 4 weeks of CPZ intoxication and 1 (=4+1) and 2 (=4+2) weeks after CPZ withdrawal. Body weight changes during the course are shown to the right. (b) Representative immunohistochemical images of myelin basic protein (MBP) and glutathione S-transferase-π (GST-π) detection in the corpus callosum in wild-type and *Nox4*$^{-/-}$ mice (scale bar, 100 μm). (c) Densitometric quantification of MBP-positive areas and GST-π–positive cells in the corpus callosum in wild-type (black) and *Nox4*$^{-/-}$ (blue) mice (n=5–17, each group). (d) Representative immunohistochemical images of proteolipid protein (PLP) and myelin-associated glycoprotein (MAG) in the corpus callosum in wild-type and *Nox4*$^{-/-}$ mice (scale bar, 100 μm) and their densitometric quantification is shown (black: wild-type and blue: *Nox4*$^{-/-}$ mice) (n=4–17, each group). (e) Quantitative PCR analysis of *Mbp* and *Mag* mRNA levels in the corpus callosum in wild-type (black) and *Nox4*$^{-/-}$ (blue) mice (n=2–5, each group). (f) Locomotor function assessed by beam walking test is shown (wild-type (black close circle), wild-type sham (black open circle), *Nox4*$^{-/-}$ (blue close triangle) and *Nox4*$^{-/-}$ sham (blue open triangle) mice (n=5, each group). Data are shown as the mean ±

SEM. (c-f): *p<0.05, †p<0.05 vs. control, one-way ANOVA followed by Bonferroni's post-hoc test.

FIGURE 2 Accumulation of oligodendrocyte precursor cells (OPCs) in the corpus callosum during the remyelination phase is significantly greater in *Nox4*$^{-/-}$ mice than that in wild-type mice. (a) Representative immunohistochemical images of platelet-derived growth factor receptor α (PDGFRα, an OPC marker) and OLIG2 (a marker of OPCs and oligodendrocytes) detection in the corpus callosum in wild-type and *Nox4*$^{-/-}$ mice (scale bar, 100 μm). (b) Densitometric quantification of PDGFRα-positive and OLIG2-positive cells in the corpus callosum in wild-type (black) and *Nox4*$^{-/-}$ (blue) mice (n=5–7, each group). (c) Cell proliferation activity assessed by immunofluorescence double-labeling of OLIG2 (green) and 5-ethynyl-2′-deoxyuridine (EdU) (red) in cultured OPCs prepared from wild-type (black) and *Nox4*$^{-/-}$ (blue) mice (n=4–5, each group; scale bar, 100 μm). Representative images (left) and quantification (right) are shown. (d) OPC proliferation, as assessed by OLIG2- and Ki67-double staining (n=7, each group), and its differentiation, as assessed by OLIG2- and APC-double staining (n=8, each group) following CPZ-induced demyelination in wild-type (black) and *Nox4*$^{-/-}$ (blue) mice. Data are shown as the mean ± SEM. (b) *p<0.05, †p<0.05 vs. control, one-way ANOVA followed by Bonferroni's post-hoc test. (c-d): *p<0.05, n.s.: not significant, unpaired t-test.

FIGURE 3 Accumulation of astrocytes positive for glial fibrillary acidic protein (GFAP) in the corpus callosum during the remyelination phase is significantly greater, and with an increased microvascular pericyte coverage, in *Nox4*$^{-/-}$ mice than that in wild-type mice. (a) Representative immunohistochemical images of GFAP detection in the corpus callosum in wild-type and *Nox4*$^{-/-}$ mice (scale bar, 100 μm). (b) Densitometric quantification of GFAP-positive areas in the corpus callosum in wild-type (black) and *Nox4*$^{-/-}$ (blue) mice (n=5–7, each group). (C) Quantitative PCR analysis of *Gfap* mRNA levels in the corpus callosum in wild-type (black) and *Nox4*$^{-/-}$ (blue) mice (n=5, each group). (d) Direct effects of CPZ (100 μM) on Nox4 expression in cultured endothelial cells and pericytes (n=6, each group) (left). Effect of CPZ on the viability of cultured pericytes (n=8, each group) (right). (e) Effects of CPZ on the intactness of the blood–brain barrier, as assessed by leakage of Evans blue dye, in wild-type mice (left) and on mRNA expression changes of *Zo-1* and *Claudin 5,* tight junction proteins, in the corpus callosum in wild-type (black) and *Nox4*$^{-/-}$ (blue) mice (n=5–6, each group). (f) Representative immunohistochemical images of collagen type IV, a basement membrane marker, and CD13, a pericyte marker, detected in the corpus callosum in wild-type and *Nox4*$^{-/-}$ mice (scale bar, 100 μm). (g) Densitometric quantification of collagen type IV-positive and CD13-positive areas in the corpus callosum in wild-type (black) and *Nox4*$^{-/-}$ (blue) mice (n=5–7, each group). (h) Quantitative PCR detection of *Ng2*

mRNA levels, a marker of neovascular pericyte as well as oligodendrocyte precursor cell (OPC), in the corpus callosum in wild-type (black) and *Nox4*$^{-/-}$ (blue) mice (n=4–5, each group). Data are shown as the mean ± SEM. (b,c,e,g,h): *p<0.05, †p<0.05 vs. control, one-way ANOVA followed by Bonferroni's post-hoc test. (d): n.s.: not significant, unpaired t-test.

FIGURE 4 Accumulation of ionized calcium-binding adapter molecule 1 (IBA1)-positive microglia and macrophages in the corpus callosum during demyelination is significantly greater in *Nox4*$^{-/-}$ mice than that in wild-type mice. (a) Representative immunohistochemical images of IBA1 detection in the corpus callosum in wild-type and *Nox4*$^{-/-}$ mice (scale bar, 100 μm). (b) Densitometric quantification of IBA1-positive areas in the corpus callosum in wild-type (black) and *Nox4*$^{-/-}$ (blue) mice (n=5–8, each group). (c) Quantitative PCR analysis of *Iba1* mRNA levels in the corpus callosum in wild-type (black) and *Nox4*$^{-/-}$ (blue) mice (n=5–7, each group). (d) Quantitative PCR analysis of *Nos2*, *Arg1*, and *C3* mRNA levels in the corpus callosum in wild-type (black) and *Nox4*$^{-/-}$ (blue) mice (n=3–7, each group). (e) Quantitative PCR analysis of *Trem2*, *Igf1*, and *Grn* mRNA levels in the corpus callosum in wild-type (black) and *Nox4*$^{-/-}$ (blue) mice (n=5–8, each group). (f) clearance of myelin debris by IBA-1-positive cells, as assessed by IBA1 and Oil red O (ORO) double staining, in the corpus callosum at four weeks in wild-type (black) and *Nox4*$^{-/-}$ (blue) mice (n=4, each group). Data are shown as the mean ± SEM. (b-e): *p<0.05, †p<0.05

vs. control, one-way ANOVA followed by Bonferroni's post-hoc test. (f): *p<0.05, unpaired t-test.

FIGURE 5 Deletion of *Nox4* enhances phagocytic capacity of cultured microglia and macrophages. (a) Reverse-transcribed PCR analysis of *Nox4* mRNA in cultured bone marrow-derived macrophages (Mø) and microglia prepared from wild-type mice. (b) Quantitative PCR analysis of changes of *Nox4* mRNA levels in cultured wild-type bone marrow-derived macrophages (BMDMs) after MD treatment (n=5, each group) (left). Quantitative PCR analysis of *Nox4* mRNA levels in the corpus callosum following CPZ administration in wild-type (black) and *Nox4*$^{-/-}$ (blue) mice (n=5–8, each group) (right). (c) Left, phagocytic capacity, assessed by immunofluorescent triple-labeling of MBP, ORO, and Hoechst, in wild-type and *Nox4*$^{-/-}$ BMDMs 48 h after MD treatment (n=4–5, each group; scale bar, 50 μm). Representative images are shown. Right, quantification of intracellular MBP-positive areas and ORO-positive areas in wild-type (black) and *Nox4*$^{-/-}$(blue) BMDMs. (d) Immunoblot analysis of total STAT3 and phosphorylated (=activated) STAT3 in wild-type (black) and *Nox4*$^{-/-}$ (blue) BMDMs after MD treatment (n=3, each group). Representative images (top) and quantification (bottom) are shown. (e) Mitochondrial membrane potential, assessed by JC-1 dye (red, hyperpolarization; green, depolarization), in wild-type and *Nox4*$^{-/-}$ BMDMs after MD treatment (n=10, each group; scale bar, 50 μm).

Representative images (left) and quantification (right) are shown. (f) Quantitative PCR analysis of changes of *Ucp2* mRNA levels after MD treatment in wild-type (black) and *Nox4*$^{-/-}$ (blue) BMDMs (n=5–6, each group). (g) Quantitative PCR analysis of changes of *Igf1* and *Grn* mRNA levels after MD treatment in wild-type (black) and *Nox4*$^{-/-}$ (blue) BMDMs (n=5–6, each group). (h) Left, phagocytic capacity, assessed by immunofluorescent triple-labeling of myelin basic protein (MBP), Oil red O (ORO), and Hoechst, in cultured wild-type (upper) and *Nox4*$^{-/-}$ (bottom) microglia 6 and 24 h after treatment with myelin debris (MD). Representative images are shown. Right, quantification of intracellular MBP-positive and ORO-positive areas (n=3–5, each group; scale bar, 50 μm). (i) Quantitative PCR analysis of changes of *Trem2*, *Igf1*, and *Grn* mRNA levels in wild-type (black) and *Nox4*$^{-/-}$(blue) microglia after MD treatment (n=4–5, each group). Data are shown as the mean ± SEM. (b,d,f,g,h,i): *p<0.05, †p<0.05 vs. control, one-way ANOVA followed by Bonferroni's post-hoc test. (c,e): *p<0.05, unpaired t-test.

FIGURE 6 Treatment with culture medium of *Nox4*$^{-/-}$ macrophages engulfing myelin debris (MD) induces the proliferation and expression of myelin basic protein (MBP) in oligodendrocyte precursor cells (OPCs). Experimental scheme for OPC proliferation and differentiation by conditioned medium of cultured bone marrow-derived macrophages (BMDMs) (a, top left) or astrocytes (b, top left) from wild-type or *Nox4*$^{-/-}$ mice. (a) Top

right, representative images of immunofluorescent triple-labeling of MBP (green), oligodendrocyte lineage transcription factor 2 (OLIG2, red), and 4′,6-diamidino-2-phenylindole (DAPI) in cultured OPCs treated with culture media of BMDMs treated with MD (MD-MCM) for 7 d (n=4–5; scale bar, 50 μm). Quantification of OLIG2-positive cells (bottom left) and MBP-positive areas among OLIG2-positive cells (bottom right). (b) Top right, representative images of immunofluorescent triple-labeling of MBP, OLIG2, and DAPI in cultured OPCs treated with culture media of astrocytes treated with MD (MD-ACM) for 7 d (n=4–5; scale bar, 50 μm). Quantification of OLIG2-positive cells (bottom left) and MBP-positive areas among OLIG2-positive cells (bottom right) (n=3–5; scale bar, 50 μm). Data are shown as the mean ± SEM. (a,b): *$p<0.05$, one-way ANOVA followed by Bonferroni's post-hoc test.